The Knee 26 (2019) 954–961

Contents lists available at ScienceDirect

The Knee

Contralateral MRI scan can be used reliably for three-dimensional meniscus sizing — Retrospective analysis of 160 healthy menisci

Silvan Beeler *, Lazaros Vlachopoulos, Lukas Jud, Reto Sutter, Philipp Fürnstahl, Sandro F. Fucentese

Department of Orthopaedics, University of Zurich, Balgrist University Hospital, Zurich, Switzerland

ARTICLE INFO

Article history:
Received 21 November 2018
Received in revised form 27 May 2019
Accepted 28 June 2019

Keywords:
Knee
Meniscus
Sizing
Allograft
3D
MRI

ABSTRACT

Background: Meniscus allograft transplantation is a valuable surgical option for post-meniscectomy syndrome. For best results, the selected allograft should be as similar as possible to the original meniscus. Three-dimensional meniscus sizing could be a new approach to improve the accuracy of meniscus matching. The contralateral anatomy might therefore be a suitable reconstruction template. The purpose of this study was to compare the three-dimensional shape of the right and left menisci by bi-planar segmentation of magnetic resonance imaging (MRI) scans.

Methods: Three-dimensional surface models of healthy menisci were created based on 40 bilateral MRI scans. Manual segmentation was performed on the MRI data in sagittal and coronal planes. For side-to-side comparison, each left meniscus model was mirrored and then superimposed to its corresponding right meniscus model. Differences between the meniscus pairs were assessed by width, length, height and surface distances. Inter-reader reliability, as well as accuracy of bi-planar segmentation was assessed by two different readers.

Results: The meniscus pairs were not significantly different in terms of width, length and height ($P =$ at least 0.138). Side difference of mean surface distances was 0.76 mm ($\pm$0.13 standard deviation (SD)) for medial and 0.78 mm ($\pm$0.15 SD) for lateral menisci. Inter-reader reliability was good to excellent (0.828–0.987).

Conclusion: The three-dimensional shapes of the left and right menisci are very similar. Therefore, the contralateral meniscus can be used as a template for three-dimensional meniscus allograft sizing. Three-dimensional meniscus segmentation and sizing can be performed accurately by combination of sagittal and coronal planes.

1. Introduction

The treatment of post-meniscectomy syndrome after subtotal or total meniscectomy in young patients is still a challenge. Recovery of the missing meniscus function by an allograft or scaffold seems to be a valid option [1]. However, the replaced meniscus should be as similar as possible to the original meniscus for optimal pressure distribution [2–4] and good clinical results [5–7]. In order to improve the restoration of the healthy anatomy, an ideal template for sizing of the missing original meniscus is desirable. Today, meniscus sizing is performed by a meniscus template consisting only of length and width, either by radiological landmarks of the ipsilateral tibial plateau in conventional radiographs [8] or by contralateral magnetic resonance imaging (MRI) scan [9,10]. Although the mean prediction values of these sizing methods are reported to be theoretically good [11], the finally received allografts from the tissue banks do often not fit well [12]. Therefore, many researchers are familiar with circumstances that give rise

* Corresponding author at: Department of Orthopaedics, Balgrist University Hospital, Forchstrasse 340, 8008 Zurich, Switzerland.
E-mail address: silvan.beeler@balgrist.ch. (S. Beeler).

https://doi.org/10.1016/j.knee.2019.06.017
0968-0160/

to serious doubts concerning the currently used sizing methods, and require a more precise technique [12,13]. These circumstances led us to introduce a new meniscus sizing method, based on the closest iterative point algorithm of three-dimensional (3D) surface models, created from an MRI scan of the healthy contralateral meniscus (Figure 1). However, this presumes that the 3D shape of the right and left menisci in an individual is similar.

Several authors demonstrated that meniscus segmentation of MRI images is feasible [14–18]. For meniscus segmentation, a slice thickness of <2 mm in a single plane is frequently used [14–16]. However, the majority of MRI scans of the knee have slice thicknesses of about 3.0 mm, similar to most standard protocols for MRI scans in our orthopaedic clinic. Because it is not economical to repeat the MRI scan with a smaller size thickness purely for the sizing, where the patient has already undergone an MRI examination, it would be preferable to develop a method of improving the quality of segmentation. Bi-planar segmentation by combination of the models created from the sagittal and coronal planes could probably improve the accuracy of the 3D models from MRI scans with greater slice thickness.

The purpose of this study was to compare right and left meniscus shapes. An equal meniscus shape could allow 3D sizing by use of a contralateral, healthy meniscus. Further we examined the feasibility of bi-planar meniscus segmentation to improve the accuracy of 3D meniscus models created from MRI images of slice thicknesses of three millimetres.

2. Materials and methods

2.1. Patients

We retrospectively analysed 40 pairs of human knee MRI scans of patients with patellofemoral disorders (20 women and 20 men) resulting in 80 medial and 80 lateral menisci. Inclusion criteria were mature skeletal age, healthy meniscus and available MRI scan of both knees. All MRI scans were performed in our clinic on a 3.0 T magnet (Skyra-fit, Siemens Healthineers, Erlangen, Germany) with a dedicated knee coil in supine position with stretched knee. The mature skeletal age was determined in MRI scans as completely closed growth plate of the femoral and tibial knee epiphyses. Meniscus integrity was assessed by an experienced musculoskeletal radiologist and any menisci with tears, degeneration or extrusion were excluded. All MRI scans had sagittal, coronal and axial reconstructions. The following sequences were acquired as part of our standard MRI protocol: (1) coronal Short Inversion Time Inversion Recovery (STIR) sequence (repetition time 4200 ms; echo time 34 ms; inversion time 210 ms; slice thickness three millimetres; number of slices 23; bandwidth 245 Hz/pixel; flip angle 150°; matrix 384 × 384; field of view 16 cm); (2) sagittal intermediate-weighted sequence with Dixon technique (repetition time 4200 ms; echo time 39 ms; slice thickness three millimetres; number of slices 30; bandwidth 250 Hz/pixel; flip angle 150; matrix 448 × 448; field of view 16 cm), with in-phase image and fat-suppressed water image; (3) axial intermediate-weighted fat-suppressed sequence coronal STIR sequence (repetition time 4990 ms; echo time 40 ms; slice thickness 2.5 mm; number of slices 39; bandwidth 150 Hz/pixel; flip angle 180°; matrix 384 × 384; field of view 15 cm).

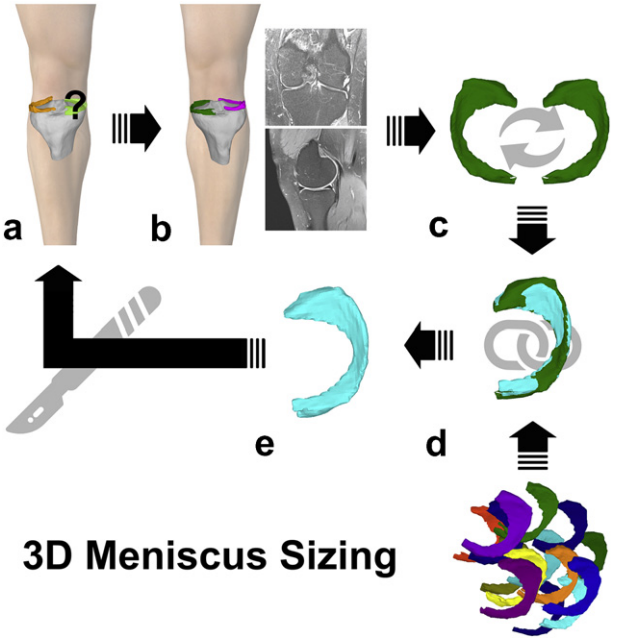

Figure 1. Three-dimensional (3D) meniscus sizing. (a) Right knee with missing medial meniscus. (b) Magnetic resonance imaging (MRI) scan of the contralateral side. (c) Meniscus segmentation and mirroring (see also Figure 2). (d) Meniscus matching by all menisci in the tissue bank by mean and maximum surface distances (see also Figure 5). (e) Selection of best-fitting meniscus for meniscus allograft surgery.

Mean age of all 40 patients was 27.5 years with a range of 15–50 years. Mean age of all 20 women was 27.2 years (range 15–47 years) and 27.8 years (range 15–50 years) for all 20 men. The mean interval between the MRI scan of the right and left knees was 10 months (range 0 to three years). Ethical approval was granted by Kantonale Ethikkommission of Zurich, Switzerland (BASEC-Nr. 2018-00856), and informed consent was obtained from all individual participants included in the study.

2.2. Meniscus segmentation

The creation of 3D surface models of the menisci from the sagittal and coronal reconstruction as well the union of the models is illustrated in Figure 2.

Meniscus segmentation was performed in a bi-planar mode (sagittal and coronal) with the Materialise Interactive Medical Control System (MIMICS) 3D reconstruction software program 18.0 (Materialise, Leuven, Belgium) (Figure 3(a)). Both menisci were segmented by manually annotating the corresponding tissue in each slice. Adjacent capsules, ligaments and tendons were excluded. Because the transverse ligament was often part of the anterior root of the medial meniscus, it was included in the segmentation until the end of the anterior meniscus root to avoid an incomplete representation of the meniscus (Figure 3(c)). The discrimination between the lateral anterior meniscus root was much easier and therefore the transverse ligament could be reliably excluded after separation of the ligament and the meniscus. Finally, the 3D models created from the sagittal and coronal reconstructions were merged with the Materialise 3-matic Medical software 11.0. In 38% of all menisci, the two parts had to be slightly realigned because of proposed small movements of the patient's knee between the sagittal and coronal MRI sequences (Figure 3(b)). The final meniscal models were then 'wrapped' (gap closing distance 0.0, smallest detail 1.0) and exported as triangular surface models for further calculations. Medial meniscus bodies were composed by an average of 2533 (1713–3249 points) surface points, and lateral meniscus bodies by an average of 2141 surface points (1626–2811 points).

2.3. Three-dimensional side-to-side evaluation

Subsequently, the 3D surface models were imported into the planning software. The left menisci were mirrored about the coronal plane. The right and corresponding mirrored left menisci were then compared according to the following criteria:

1) Measurement of length, width and height. Length, width and height were measured in a standardized fashion. First, an oriented bounding box (OBB) was calculated from all model points [19]. The OBB is the minimal-volume rectangular box fully enclosing the meniscal model. The box was then rotated around the *z*-axis (Figure 4, blue axis) until the *x*-axis (Figure 4, red axis) was parallel to the tips of the anterior and posterior meniscus roots. The box was then adjusted in length, width and height, such that the meniscus was best surrounded by the box. Length (*x*-axis), width (*y*-axis) and height (*z*-axis) are represented by the lengths of the box.
2) Quantification of the similarity of the meniscal model surfaces. For the quantification of the similarity of the surface models, we analysed the distances between the model points of the superimposed menisci of both sides. First, the mirrored left meniscal model was automatically superimposed with the corresponding right model using the iterative closest point (ICP)

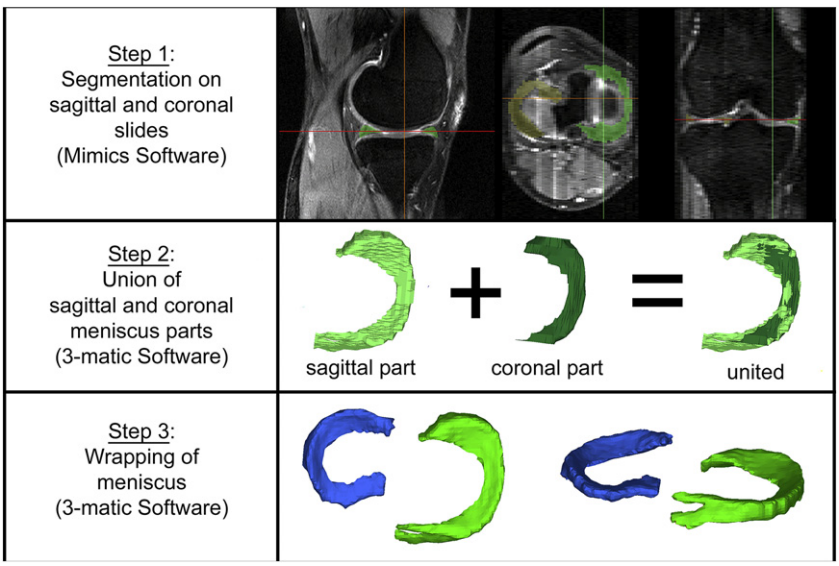

Figure 2. Meniscus segmentation. (a) Step 1: segmentation was performed in sagittal and coronal slides by manual annotation of all meniscus tissue. (b) Step 2: three-dimensional (3D) sagittal and coronal meniscus parts were merged. In cases when there was a shift due to the patient's movement during acquisition of the different reconstructions, manual realignment had to be performed first. (c) Step 3: wrapping of the meniscus surface was performed by 3-matic software.

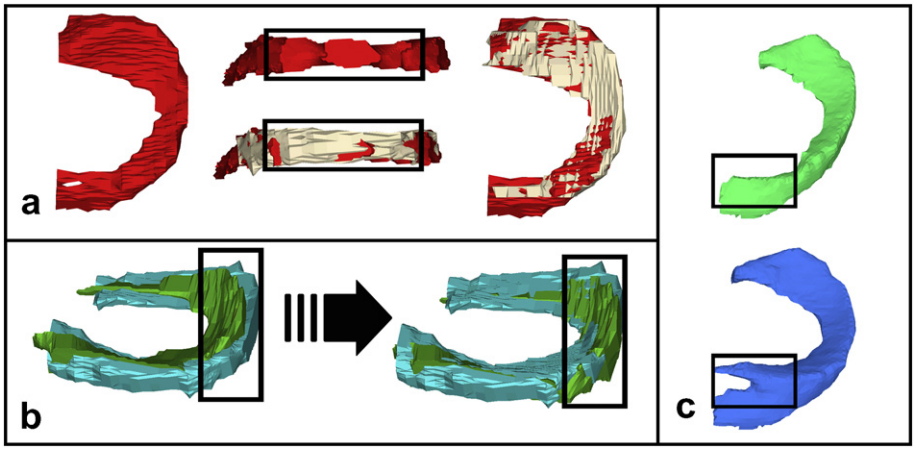

Figure 3. Rationality of segmentation in coronal and sagittal plane. (a) Inaccuracy of the intermediate part of the meniscus with segmentation only in sagittal slices (red meniscus). Improvement by combination of sagittal and coronal (light brown meniscus) slices. (b) Inaccuracy of sagittal and coronal meniscus parts because of motion artefacts. Improvement by manual correction. (c) Incomplete anterior medial meniscus root by absent transverse ligament. Complete anterior meniscus root with present transverse ligament.

algorithm [20,21] (Figure 5(a)). Thereafter, we calculated the (mean and maximum) distances of all surface points of one model to the closest points of the second model (right-to-left and left-to-right (Figure 5(b))). For further calculations, the mean of all points (right-to-left and left-to-right) and the maximum distance of right-to-left and left-to-right were used. Hereby, two 3D meniscal models could be compared by the mean and maximum distances of their surface points as well as by the Hausdorff distance [22–26]. The Hausdorff distance is a suitable measurement method of boundary similarity between two objects and is frequently used for video sequences matching [22], facial recognition [23] and for evaluating the performance of medical segmentation and image registration [24–26].

3) Outliers of all surface points with a distance of more than two millimetres and three millimetres. We defined as 'outliers' the percentage of surface points with a distance of more than two millimetres and three millimetres, respectively, from the nearest points of the corresponding model. To this end we calculated first a distance map of all surface points and analysed the results using the ParaView Software 5.5.0. For further calculations, only the larger values of right-to-left and left-to-right were used according to the Hausdorff method [22–26].
4) Error location of surface points with a distance of more than three millimetres. To analyse the location of the highest errors, the meniscus body was separated into eight zones, as illustrated in Figure 6. All surface points with a distance of more than three millimetres were allocated to the previously introduced zones and rated with one point if they exceeded the three millimetres. Finally, the percentage of the maximum possible value of 40 points (=40 different menisci) was calculated.

2.4. Reliability of bi-planar meniscus segmentation

Two readers created 3D triangular surface models with the previously described bi-planar segmentation (sagittal and coronal with following merging) independently of 20 meniscus pairs for inter-reader reliability. Further, the first reader repeated the segmentation after one month for intra-reader reliability. Comparison was carried out by mean differences of all surface points and interclass correlation (ICC) of meniscus width, length and height.

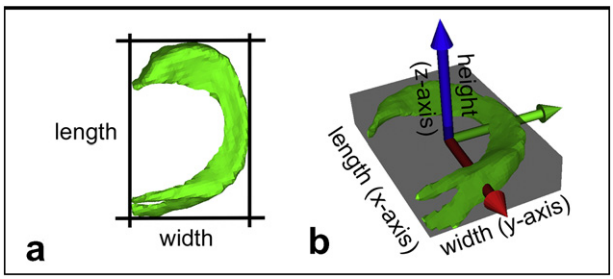

Figure 4. Measurement of length, width and height. (a) A best fitting three-dimensional (3D) box was placed around the meniscus. The *x*-axis was parallel to a line between anterior and posterior meniscus root. (b) *x*-axis = meniscus length, *y*-axis = meniscus width, *z*-axis = meniscus height.

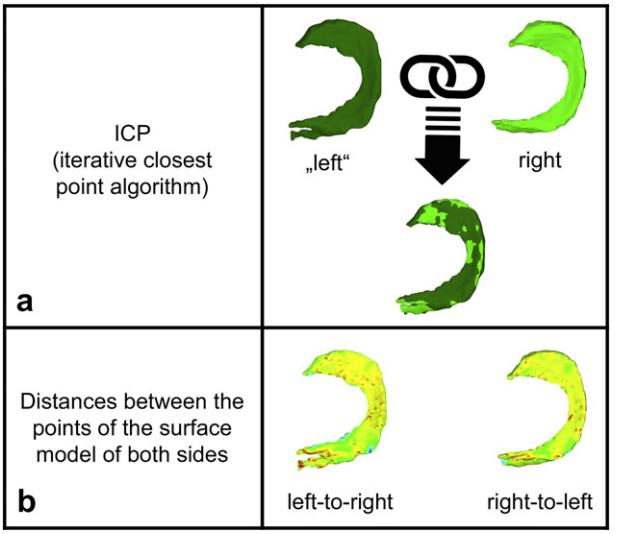

Figure 5. Measurement mean/maximum surface distances. (a) Mirrored left meniscus ('left') is superimposed with the right meniscus ('right') using the iterative closed-point algorithm (ICP). (b) The mean and maximum differences of all surface points to the closest points of the corresponding model are calculated. In this example, left-to-right (L-R) agreement = mean 0.70, max 2.37. Right-to-left (R-L) agreement = mean 0.86, max 4.23. Overall agreement (highest values of both) = mean 0.86, max 4.23.

2.5. Statistics

Normal distribution of our data was validated with the Kolmogorov–Smirnov test. The mean, standard deviation, median, and range (min/max) were calculated from the absolute values. Right–left (R/L) differences were calculated as difference from the right to the left values. Student's *t*-test was conducted to evaluate overall differences in morphometric dimensions between right and left knees. Significance was set at $P < 0.05$.

3. Results

3.1. 3D side-to-side evaluation

1) Length, width and height. There were no significant differences between left and right meniscus dimensions according to 3D measured meniscus width, length and height. All results are listed in Table 1.
2) Mean/maximum surface distances. Mean distance between all surface points of left and right menisci was 0.76 mm for medial and 0.78 mm for lateral meniscus. All results are listed in Table 2.
3) Outliers of all surface points with a distance of more than two millimetres and three millimetres; 1.6% (medial meniscus), respectively, 1.3% (lateral meniscus) of all surface points had a distance of more than three millimetres. All results are listed in Table 2.

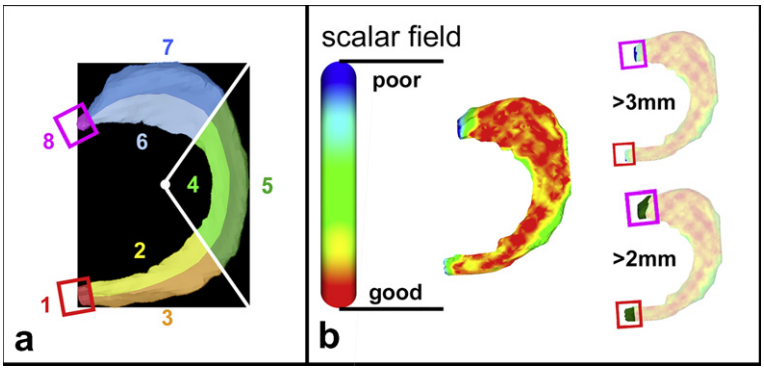

Figure 6. Zones of error location. (a) Medial and lateral menisci were divided into eight zones. Zone 1 = tip of anterior meniscus root, Zone 2 = inner part of anterior third, Zone 3 = outer part of anterior third, Zone 4 = inner part of middle third, Zone 5 = outer part of middle third, Zone 6 = inner part of posterior third, Zone 7 = outer part of posterior third, Zone 8 = tip of posterior meniscus root. (b) Scalar field shows differences of the meniscus surface points. Red = closest, Blue = furthest. Surface points with a distance of more than two millimetres and three millimetres are illustrated in Zones 1 and 8.

Table 1
Side differences: length, width and height.

	Width		Length		Height	
	R	L	R	L	R	L
Medial meniscus						
Mean (mm)	31.9	33.0	47.2	47.2	9.71	9.62
Min/max (mm)	24.2–37.7	26.2–39.8	36.2–52.6	34.5–53.0	6.3–13.5	7.2–11.9
Standard deviation (SD)	3.17	3.34	3.78	3.63	1.44	1.28
Right–left (R/L) differences						
Mean difference R/L (mm)	2.22		1.64		0.86	
Max difference R/L (mm)	6.80		5.40		4.30	
Standard deviation R/L	1.36		1.13		0.81	
Significance R ≠ L (*P* value)	0.138		0.836		0.756	
Lateral meniscus						
Mean (mm)	32.5	32.0	35.8	35.6	10.3	10.1
Min/max (mm)	27.5–39.2	26.4–43.2	31.1–42.6	31.3–41.8	8.1–14.0	7.4–14.9
Standard deviation (SD)	3.55	4.29	2.95	2.79	1.49	1.50
Right–left (R/L) differences						
Mean difference R/L (mm)	1.71		1.64		0.95	
Max difference R/L (mm)	5.50		5.70		3.10	
Standard deviation R/L	1.40		1.38		0.78	
Significance R ≠ L (*P* value)	0.576		0.736		0.426	

4) Error location of surface points with a distance of more than three millimetres. Main error locations were the tips of both menisci. With 70%, the tip of the anterior medial meniscus root was most commonly affected, followed by the tip of the anterior lateral meniscus root (42.5%), tip of the posterior medial (37.5%) and lateral (27.5%) meniscus root. Least affected was the medial third of both menisci and the inner part of the posterior third. All results are listed in Table 3.

3.2. Reliability of bi-planar meniscus segmentation

Inter- and intra-reader reliability was excellent for meniscus width and length (ICC at least 0.913). Meniscus height showed good inter-reader and excellent intra-reader reliability. Mean surface distance between two different readers was on average 0.53 mm for medial and 0.59 mm for lateral meniscus. All values are given in Table 4.

4. Discussion

To our knowledge, this is the first study to compare the 3D shape of right and left menisci according to the surface distance. Thus far, side-to-side comparison of the meniscus shape has only been performed two-dimensionally by meniscus length, width and height [27–29]. Although these studies were able to find good correlations between right and left sides, 3D shape comparison by all surface points is needed for 3D meniscus sizing to ascertain how accurate sizing with the contralateral side can be. Generally, mean and maximum surface distances have to be as low as possible for best agreement. Our study shows that mean values around 0.76–0.78 mm (±0.125–0.149 standard deviation (SD)) and maximum values around 3.35–3.44 mm (±0.718–0.829 SD) have to be expected by sizing with the contralateral side on bi-planar segmentation.

Although sagittal slices were best suitable for meniscus segmentation [14–18], the medial and lateral ends could often not adequately be segmented due to lower partial volume effects, a higher contrast-to-noise ratio for meniscus and surrounding tissues in the joint periphery and/or wide slice thicknesses up to three millimetres. Bi-planar segmentation by combination of the sagittal and coronal planes could improve the 3D shape accuracy, despite slice thicknesses of up to three millimetres. Therefore, already performed MRI sequences with wide slice thickness can be used for 3D meniscus sizing by manual bi-planar segmentation.

Table 2
Side differences: surface points.

	Mean surface difference	Maximal surface difference	>2 mm % Pt difference	>3 mm % Pt difference
Medial meniscus				
Mean/median (mm)	0.76/0.76	3.44/3.63	3.9/3.3	1.6/0.6
Range (mm) (min/max)	0.5 (0.5–1.0)	3.88 (1.8–5.6)	13.1 (0–13.1)	16.0 (0–16)
Standard deviation	0.125	0.829	2.95	2.90
Lateral meniscus				
Mean/median (mm)	0.78/0.78	3.35/3.26	4.8/3.4	1.3/0.4
Range (mm) (min/max)	0.68 (0.5–1.2)	3.42 (1.8–5.2)	19 (0–19)	11.9 (0–11.9)
Standard deviation	0.149	0.718	4.23	2.66

Table 3
Zones of error location.

	Medial meniscus	Lateral meniscus
Zone 1	70%	42.5%
Zone 2	2.5%	2.5%
Zone 3	17.5%	20%
Zone 4	10%	2.5%
Zone 5	0%	15%
Zone 6	0%	0%
Zone 7	7.5%	7.5%
Zone 8	37.5%	27.5%

This study has a few limitations. A slice thickness of up to three millimetres can falsify the results of side-to-side comparison. Because of the retrospective design of the study, it was not possible to have enough bilateral MRI scans with smaller slice thicknesses. However, it was also the aim of the study to find out whether the sizing in a standard three-millimetre MRI protocol is feasible. We reduced this problem of three-millimetre slices by bi-planar segmentation. We could confirm that in a bi-planar segmentation of three-millimetre slices an accurate sizing can be achieved. A problem with the bi-planar segmentation was that patients could move their knees slightly between the two sequences. Therefore, slight manual correction of the sagittal and coronal meniscus parts is needed before merging. Overall, reconstruction of a 3D meniscus by this technique works very well with excellent intra- and inter-reader reliability. A second limitation was the fact, that we only analysed patients with patellofemoral disorders. These patients often have bilateral problems of the knee – and therefore often available bilateral MRI scans in our database – and often no concomitant meniscal tears. Although our results are in the narrow sense only valid for patients with patellofemoral disorders, we do not see that as a relevant limitation because the tibiofemoral joint with its menisci is in general not correlated to that pathology [30].

Three-dimensional meniscus sizing has some great advantages. Not only can the best fitting 3D meniscus be found by this method, but, if desired, a slightly greater size because of presumed meniscus shrinkage, as also slightly smaller size because of presumed extrusion can be easily ordered by down- or up-scaling of the 3D template [31]. This depends on the surgeon's preferences. It might be reasonably assumed that a 3D equal shape of the meniscus could also improve the feasibility of 'bone plugs' or 'bone bridge' fixation methods [2], which are supposed to be superior to 'soft-tissue' and 'suture bone tunnel' fixation techniques [2]. Although not established, this template could also be used for biomimetic 3D-printed scaffolds [32,33].

However, 3D meniscus sizing can only be performed if the tissue banks are willing to offer this option, which involves additional costs. All of their meniscus allografts have to be scanned and three-dimensionally reconstructed. This reconstruction could probably be partly or fully automated [34,35], which would entail additional costs. Further, specific software needs to be developed, which allows automated comparison of the meniscus template of the healthy contralateral meniscus with all available allografts in the database of the tissue bank. However, even if all this is possible, the proof of this additional effort has first to be

Table 4
Inter-/intra-reader reliability.

Medial meniscus (n = 20)						
	Width		Length		Height	
ICC_{inter}/ICC_{intra}	0.948	0.987	0.913	0.974	0.828	0.957
Medial meniscus (n = 20)						
	Mean surface distance difference				Max surface distance difference	
Mean ± SD	0.53 ± 0.084				2.42 ± 0.570	
Range (min/max)	0.34 (0.35–0.69)				1.86 (1.49–3.35)	
Lateral meniscus (n = 20)						
	Width		Length		Height	
ICC_{inter}/ICC_{intra}	0.951	0.955	0.973	0.977	0.911	0.940
Lateral meniscus (n = 20)						
	Mean surface distance difference				Max surface distance difference	
Mean ± SD	0.59 ± 0.045				2.66 ± 0.911	
Range (min/max)	0.16 (0.51–0.67)				4.09 (1.44–5.53)	

ICC, interclass correlation; SD, standard deviation.

evaluated compared with the conventional sizing methods according to two-dimensional meniscus width and length. Further studies will be necessary to analyse, for example, whether the contralateral MRI should be preferred compared to conventional X-ray- or computed-tomography-based sizing.

5. Conclusion

The intra-individual 3D shapes of left and right menisci are very similar. Therefore, the contralateral side can be used as a template for 3D meniscus allograft sizing.

Three-dimensional meniscus segmentation and sizing can be performed accurately with MRI sequences of slice thickness up to three millimetres by combination of sagittal and coronal planes (bi-planar).

Declaration of Competing Interest

None declared.

References

[1] Ryu RK, Dunbar VW, Morse GG. Meniscal allograft replacement: a 1-year to 6-year experience. Arthroscopy 2002;18:989–94.
[2] Rodeo SA. Meniscal allografts—where do we stand? Am J Sports Med 2001;29:246–61.
[3] Haut Donahue TL, Hull ML, Rashid MM, Jacobs CR. The sensitivity of tibiofemoral contact pressure to the size and shape of the lateral and medial menisci. J Orthop Res 2004;22:807–14.
[4] Huang A, Hull ML, Howell SM, Haut Donahue T. Identification of cross-sectional parameters of lateral meniscal allografts that predict tibial contact pressure in human cadaveric knees. J Biomech Eng 2002;124:481–9.
[5] Cameron JC, Saha S. Meniscal allograft transplantation for unicompartmental arthritis of the knee. Clin Orthop Relat Res 1997:164–71.
[6] Rath E, Richmond JC, Yassir W, Albright JD, Gundogan F. Meniscal allograft transplantation. Two- to eight-year results. Am J Sports Med 2001;29:410–4.
[7] van Arkel ER, de Boer HH. Survival analysis of human meniscal transplantations. J Bone Joint Surg Br 2002;84:227–31.
[8] Papalia R, Del Buono A, Osti L, Denaro V, Maffulli N. Meniscectomy as a risk factor for knee osteoarthritis: a systematic review. Br Med Bull 2011;99:89–106.
[9] Donahue TL, Hull ML, Howell SM. New algorithm for selecting meniscal allografts that best match the size and shape of the damaged meniscus. J Orthop Res 2006; 24:1535–43.
[10] Haut TL, Hull ML, Howell SM. Use of roentgenography and magnetic resonance imaging to predict meniscal geometry determined with a three-dimensional coordinate digitizing system. J Orthop Res 2000;18:228–37.
[11] Cox JS, Nye CE, Schaefer WW, Woodstein IJ. The degenerative effects of partial and total resection of the medial meniscus in dogs' knees. Clin Orthop Relat Res 1975:178–83.
[12] Stevenson C, Mahmoud A, Tudor F, Myers P. Meniscal allograft transplantation: undersizing grafts can lead to increased rates of clinical and mechanical failure. Knee Surg Sports Traumatol Arthrosc 2019;27:1900–7.
[13] Haen TX, Boisrenoult P, Steltzlen C, Pujol N. Meniscal sizing before allograft: comparison of three imaging techniques. Knee 2018;25:841–8.
[14] Stone KR, Stoller DW, Irving SG, Elmquist C, Gildengorin G. 3D MRI volume sizing of knee meniscus cartilage. Arthroscopy 1994;10:641–4.
[15] Bowers ME, Tung GA, Fleming BC, Crisco JJ, Rey J. Quantification of meniscal volume by segmentation of 3T magnetic resonance images. J Biomech 2007;40: 2811–5.
[16] Bloecker K, Wirth W, Guermazi A, Hunter DJ, Resch H, Hochreiter J, et al. Relationship between medial meniscal extrusion and cartilage loss in specific femorotibial subregions: data from the Osteoarthritis Initiative. Arthritis Care Res 2015;67:1545–52.
[17] Kruger N, McNally E, Al-Ali S, Rout R, Rees JL, Price AJ. Three-dimensional reconstructed magnetic resonance scans: accuracy in identifying and defining knee meniscal tears. World J Orthop 2016;7:731–7.
[18] Wirth W, Frobell RB, Souza RB, Li X, Wyman BT, Le Graverand MP, et al. A three-dimensional quantitative method to measure meniscus shape, position, and signal intensity using MR images: a pilot study and preliminary results in knee osteoarthritis. Magn Reson Med 2010;63:1162–71.
[19] Schneider PJ, Eberly DH. Geometric tools for computer graphics; 2003.
[20] Audette MA, Ferrie FP, Peters TM. An algorithmic overview of surface registration techniques for medical imaging. Med Image Anal 2000;4:201–17.
[21] Chen Y, Medioni G. Object modeling by registration of multiple range images. Proceedings 1991 IEEE International Conference on Robotics and Automation; 1991. p. 2724–9 [vol.3].
[22] Sang Hyun K, Rae-Hong P. An efficient algorithm for video sequence matching using the modified Hausdorff distance and the directed divergence. IEEE Trans Circuits Syst Video Technol 2002;12:592–6.
[23] Gao Y. Efficiently comparing face images using a modified Hausdorff distance. IEE Proceedings Vision, Image and Signal Processing 2003;150:346–50.
[24] Morain-Nicolier F, Lebonvallet S, Baudrier E, Ruan S. Hausdorff distance based 3D quantification of brain tumor evolution from MRI images. 2007 29th Annual International Conference of the IEEE Engineering in Medicine and Biology Society; 2007. p. 5597–600.
[25] Tang M, Lee M, Kim YJ, et al. J ACM Trans Graph 2009;28:1–9.
[26] Ghaffari M, Sanchez L, Xu G, Alaraj A, Zhou XJ, Charbel FT, et al. Validation of parametric mesh generation for subject-specific cerebroarterial trees using modified Hausdorff distance metrics. Comput Biol Med 2018;100:209–20.
[27] Prodromos CC, Joyce BT, Keller BL, Murphy BJ, Shi K. Magnetic resonance imaging measurement of the contralateral normal meniscus is a more accurate method of determining meniscal allograft size than radiographic measurement of the recipient tibial plateau. Arthroscopy 2007;23:1174–1179.e1.
[28] Yoon JR, Jeong HI, Seo MJ, Jang KM, Oh SR, Song S, et al. The use of contralateral knee magnetic resonance imaging to predict meniscal size during meniscal allograft transplantation. Arthroscopy 2014;30:1287–93.
[29] Dargel J, Feiser J, Gotter M, Pennig D, Koebke J. Side differences in the anatomy of human knee joints. Knee Surg Sports Traumatol Arthrosc 2009;17:1368–76.
[30] Iwano T, Kurosawa H, Tokuyama H, Hoshikawa Y. Roentgenographic and clinical findings of patellofemoral osteoarthrosis. With special reference to its relationship to femorotibial osteoarthrosis and etiologic factors. Clin Orthop Relat Res 1990:190–7.
[31] Samitier G, Alentorn-Geli E, Taylor DC, Rill B, Lock T, Moutzouros V, et al. Meniscal allograft transplantation. Part 1: systematic review of graft biology, graft shrinkage, graft extrusion, graft sizing, and graft fixation. Knee Surg Sports Traumatol Arthrosc 2015;23:310–22.
[32] Szojka A, Lalh K, Andrews SHJ, Jomha NM, Osswald M, Adesida AB. Biomimetic 3D printed scaffolds for meniscus tissue engineering. Bioprinting 2017;8:1–7.
[33] Zhang ZZ, Wang SJ, Zhang JY, Jiang WB, Huang AB, Qi YS, et al. 3D-printed poly(epsilon-caprolactone) scaffold augmented with mesenchymal stem cells for total meniscal substitution: a 12- and 24-week animal study in a rabbit model. Am J Sports Med 2017;45:1497–511.
[34] Paproki A, Engstrom C, Chandra SS, Neubert A, Fripp J, Crozier S. Automated segmentation and analysis of normal and osteoarthritic knee menisci from magnetic resonance images—data from the Osteoarthritis Initiative. Osteoarthr Cartil 2014;22:1259–70.
[35] Dam EB, Lillholm M, Marques J, Nielsen M. Automatic segmentation of high- and low-field knee MRIs using knee image quantification with data from the osteoarthritis initiative. J Med Imaging 2015;2:024001.